ACS OMEGA

Article

http://pubs.acs.org/journal/acsodf

Electroless Deposition and Ignition Properties of Si/Fe_2O_3 Core/Shell Nanothermites

Sidi Huang,[†,§] Sili Deng,[†,§] Yue Jiang,[‡] Jiheng Zhao,[†] and Xiaolin Zheng*[,†]

[†]Department of Mechanical Engineering and [‡]Department of Materials Science and Engineering, Stanford University, Stanford, California 94305, United States

ABSTRACT: Thermite, a composite of metal and metal oxide, finds wide applications in power and thermal generation systems that require high-energy density. Most of the researches on thermites have focused on using aluminum (Al) particles as the fuel. However, Al particles are sensitive to electrostatic discharge, friction, and mechanical impact, imposing a challenge for the safe handling and storage of Al-based thermites. Silicon (Si) is another attractive fuel for thermites because of its high-energy content, thin native oxide layer, and facile surface functionality. Several studies showed that the combustion properties of Si-based thermites are comparable to those of Al-based thermites. However, little is known about the ignition properties of Si-based thermites. In this work, we determined the reaction onset temperatures of mechanically mixed (MM) Si/Fe_2O_3 nanothermites and Si/Fe_2O_3 core/shell (CS) nanothermites using differential scanning calorimetry. The Si/Fe_2O_3 CS nanothermites were prepared by an electroless deposition method. We found that the Si/Fe_2O_3 CS nanoparticles (NPs) had a lower reaction onset temperature (~550 °C) than the MM Si/Fe_2O_3 nanothermites (>650 °C). The onset temperature of the Si/Fe_2O_3 CS nanothermites is also insensitive to the size of the Si core NP. These results indicate that the interfacial contact quality between Si and Fe_2O_3 is the dominant factor for determining the ignition properties of thermites. Finally, the reaction onset temperature of the Si/Fe_2O_3 CS NPs is comparable to that of the commonly used Al-based nanothermites, suggesting that Si is an attractive fuel for thermites.

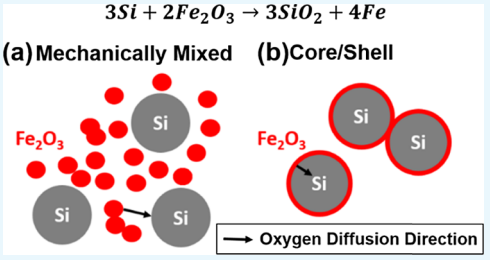

INTRODUCTION

Thermite is an energetic composite of metals as fuels (e.g., Al, B, and Si) and metal oxides as oxidizers (e.g., CuO, Fe_2O_3, and WO_3). Once ignited, thermite releases a large amount of heat and thus finds applications, ranging from aerospace propulsion, thermal batteries, waste disposals, and power generation for microsystems to material synthesis.[1−4] Most of the researches on thermites have focused on using aluminum (Al) as the fuel.[5−11] However, Al, especially Al nanoparticles (Al NPs), is sensitive to electrostatic discharge, friction, and mechanical impact,[12] imposing a challenge for the safe handling and storage of Al-based thermites. In addition, Al particles have a native oxide layer of 2−6 nm, which acts as a dead mass.[13] Among other fuels such as red phosphorus[14] and boron,[15,16] silicon (Si) is another attractive fuel for thermites because it has high volumetric and specific energy densities (75.1 MJ/L and 32.2 MJ/kg, respectively) similar to those of Al (83.8 MJ/L and 31.0 MJ/kg, respectively). Si also has a thinner native oxide layer of 1−3 nm than Al,[17] and it is resistant to electrostatic discharge. Importantly, the surface of Si can be easily functionalized,[18,19] facilitating the use of coating and surface modification to tailor its ignition and burning properties. Several previous studies have shown that Si-based thermites have comparable combustion properties as Al-based thermites,[18,20,21] in terms of adiabatic combustion temperatures (~3000 K) and burning rates (40−530 m/s).[22] However, little is known about the ignition properties of Si-based thermites and their dependence on the structure of thermites.

Herein, we study the ignition properties, in terms of reaction onset temperatures, of Si and Fe_2O_3 thermite mixtures. The reason for choosing Fe_2O_3 as the oxidizer is that Al/Fe_2O_3 is one of the most studied thermite systems.[23] Moreover, the thermite reaction between Si and Fe_2O_3 ($3Si + 2Fe_2O_3 \rightarrow 3SiO_2 + 4Fe$, 12.9 MJ/kg of Si) has the least amount of gaseous byproducts among thermites,[20] allowing us to focus on the structural effect on the oxygen diffusion process that is critical to ignition. In particular, we compared the reaction onset temperatures of Si/Fe_2O_3 core/shell (CS) particles with those of the mechanically mixed (MM) Si/Fe_2O_3 powders (Figure 1). We found that the Si/Fe_2O_3 CS NPs had a lower reaction onset temperature (~550 °C) than the MM Si/Fe_2O_3 nanothermites (>650 °C). These results indicate that the interfacial contact quality between Si and Fe_2O_3 is the dominant factor for determining the ignition properties of thermites, a phenomenon similar to that in Al-based thermites.[3] Finally, the reaction onset temperature of the Si/Fe_2O_3 CS NPs is comparable to that of the commonly used Al-based nanothermites, suggesting that Si is an attractive fuel for thermites.

We investigated the ignition properties of Si/Fe_2O_3 nanothermites by using Si NPs of two different sizes (20−30 nm, US Research Nanomaterials, and 100 nm, Skyspring Nanomaterials Inc.). The oxygen content of these particles is summarized in Table 1. Overall, the oxygen content of both sizes of Si NPs is

Received: May 23, 2017
Accepted: July 4, 2017
Published: July 13, 2017

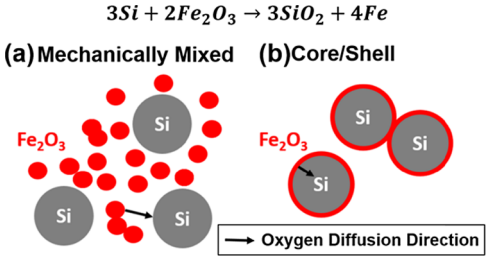

Figure 1. Schematics of (a) MM and (b) CS Si/Fe_2O_3 thermites. The improved contact between Si and Fe_2O_3 in the CS structure facilitates the oxygen diffusion process and hence lowers the reaction onset temperature.

Table 1. Oxygen Contents of Different Si Particles

material	oxygen content (wt %)	references
20−30 nm Si	0.81	26
100 nm Si	0.50	27

negligible. The MM Si/Fe_2O_3 samples (Figure 1a) were prepared by dispersing 100 mg of Si and 380.2 mg of Fe_2O_3 into 10 mL of hexane, followed by sonication for 30 min and drying on a hot plate at 100 °C. The Si/Fe_2O_3 CS NPs (Figure 1b) were prepared by coating Si with an Fe_2O_3 shell using an electroless deposition method.[24] As schematically illustrated in Figure 2a, the Si particles were first coated with a Pd layer through electrostatic plating. Then, Pd was replaced by Fe through electroless plating. The formed Si/Fe NPs were converted to Si/Fe_2O_3 CS NPs by thermal annealing. The detailed synthesis process is described in the Methods section.

RESULTS AND DISCUSSION

The scanning electron microscopy (SEM) images in Figure 2b−e show the representative morphologies of the initial Si particles (Figure 2b,c, average diameter: 100 nm) and the final coated Si/Fe_2O_3 NPs (Figure 2d,e). The surface of the initial Si particles is smooth (Figure 2c), and it becomes rather rough after the synthesis (Figure 2e), indicating a successful coating. SEM inspection over a wide range of samples shows that the surface of the Si particle is coated with a shell. The coating of Fe_2O_3 over the Si surface is also confirmed by transmission electron microscopy (TEM) and energy-dispersive X-ray spectroscopy (EDXS) mapping. It should be noted that the SEM images were taken for the 100 nm Si NPs because of the spatial resolution limit and that the TEM images were taken for 20−30 nm Si particles for better electron transmission. Both the TEM and standing TEM (STEM) images (Figure 3a,b) suggest that the final particle has a CS structure. The EDXS element mapping of the boxed regime in Figure 3a shows the coexistence of strong Fe element and O element signals and relatively weak Si signals, indicating that a layer of Fe_2O_3 has been deposited on the surface of Si. However, because the initial sizes and shapes of Si particle have an inherent distribution, it is difficult to determine the exact thickness of iron oxide. Instead, we have estimated the Si/Fe_2O_3 equivalence ratios using an inductively coupled plasma optical emission spectroscopy (Thermo Scientific ICAP 6300 Duo view spectrometer) system. The estimated equivalence ratios of 20−30 nm and 100 nm Si/Fe_2O_3 CS particles are 24.1 ± 0.15 and 6.07 ± 0.02, respectively. In addition, the X-ray photoelectron spectroscopy (XPS) analysis of the Si/Fe_2O_3 CS NP in Figure 3f shows the characteristic iron oxide peaks (Fe $2p_{3/2}$ and Fe $2p_{1/2}$, 711.4 and 724.2 eV, respectively), confirming the shell chemical composition of Fe_2O_3. Finally, the X-ray diffraction (XRD) analysis of both the Si/Fe_2O_3 CS and MM NPs shows the characteristic peaks of Si and Fe_2O_3 (Figure 3g). The above characterizations indicate that we have synthesized Si/Fe_2O_3 CS NPs.

Next, we used differential scanning calorimetry (DSC) to determine the reaction onset temperatures of Si/Fe_2O_3 CS NPs and compare with those of the MM NPs. Figure 4 shows the representative baseline-corrected DSC profiles of Si/Fe_2O_3 CS and MM samples with two different sizes of the Si particle. First, the onset temperature of the Si/Fe_2O_3 CS NPs is about 550 °C, which is about 100−150 °C lower than that of the MM samples. This confirms that the CS structure has more facile oxygen diffusion process because of its better interfacial contact between Si and Fe_2O_3. Second, the onset temperature of the 20 nm Si/Fe_2O_3 (MM) is about 50 °C lower than that of the 100 nm Si/Fe_2O_3 (MM), confirming the importance of size effect. A smaller size NP has a larger specific surface area and a shorter diffusion distance for oxygen, and both factors contribute to the lower onset temperature. By contrast, the onset temperature of the 20 nm Si/Fe_2O_3 (CS) is about the same as that of the 100 nm Si/Fe_2O_3 (CS), indicating that intimate interfacial contact between Si and Fe_2O_3 in the CS structure has already effectively minimized the oxygen diffusion length. Hence, the initial size of the Si NP plays a negligible role here. In other words, the reaction onset temperature of Si/Fe_2O_3 nanothermites is mostly affected by their interfacial contact quality.

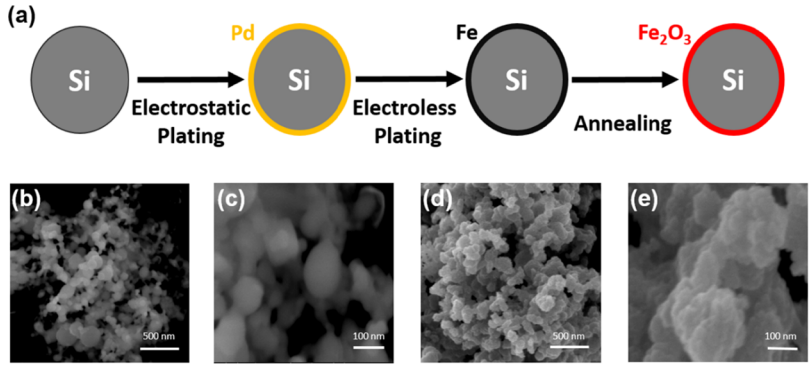

Figure 2. (a) Schematics of the electroless deposition process to coat Si NPs with Fe_2O_3 shells; SEM images of (b) initial Si NPs (100 nm); (c) magnification of (b); (d) Si/Fe_2O_3 CS NPs; and (e) magnification of (d).

DOI: 10.1021/acsomega.7b00652
ACS Omega 2017, 2, 3596−3600

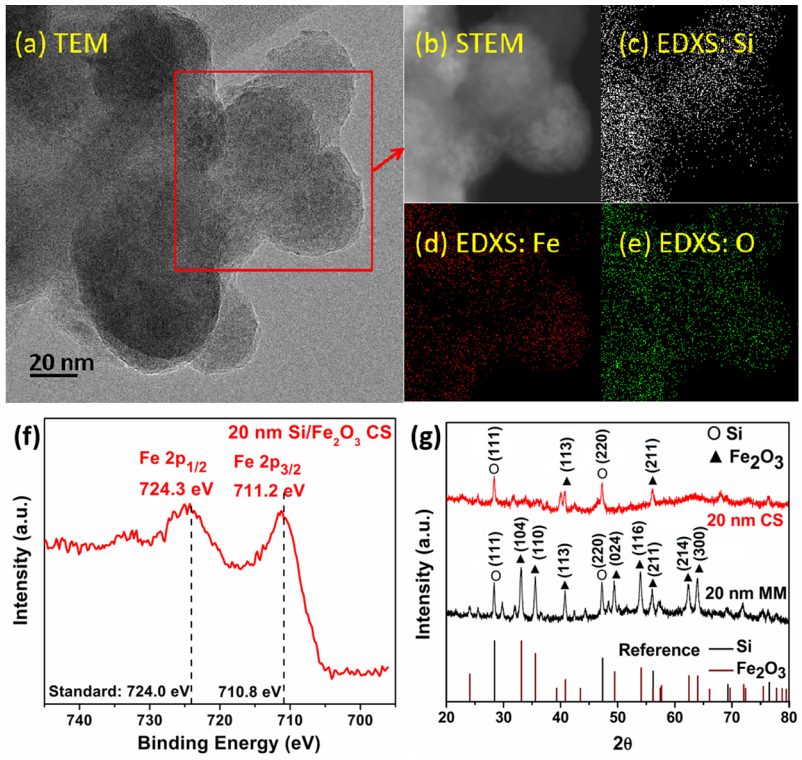

Figure 3. Material characterization of Si (20 nm)/Fe_2O_3 CS NPs: (a) TEM image; (b) STEM image of the boxed region in (a); EDXS mapping of (c) Si, (d) Fe, and (e) O elements in the boxed region in (a); (f) XPS spectra; and (g) XRD in comparison with that of Si/Fe_2O_3 MM NPs. These characterizations confirm the formation of Si/Fe_2O_3 CS NPs.

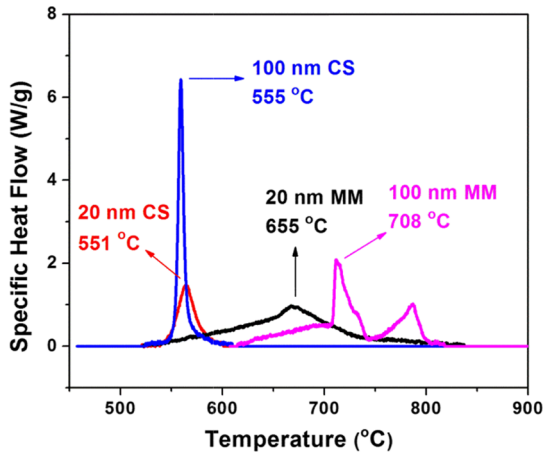

Figure 4. Baseline-corrected DSC traces of Si/Fe_2O_3 CS NPs and MM samples for two different initial sizes of Si particles (20 and 100 nm).

Finally, we compared the reaction onset temperatures of our Si/Fe_2O_3 CS NPs with those of Al/metal oxide nanothermites in the literature. We chose the Al/metal oxide nanothermites that have comparable Al size with our Si NPs for fair comparison, and the results are listed in Table 2. It is clear that Si/Fe_2O_3 CS NPs have comparable reaction onset temperatures as other Al/metal oxide nanothermites (460–580 °C). These data suggest that replacing Al with Si in thermites will have little change in terms of reaction onset temperatures.

CONCLUSIONS

We have shown that the easy surface functionality of Si allows a facile synthesis of Si/Fe_2O_3 CS NPs using a simple electroless plating method. The formed Si/Fe_2O_3 CS NPs have a reaction onset temperature of about 550 °C, which is about 100–150 °C lower than that of the MM samples. The lowering of the reaction onset temperature is caused by the enhanced intermolecular oxygen diffusion processes in the CS structure. In addition, the reaction onset temperature of the Si/Fe_2O_3 CS NPs is comparable to that of the commonly used Al-based nanothermites. Considering the easy surface functionalization property and comparable ignition properties, our study suggests that Si is another attractive fuel for thermites. Our synthesis methodology can be applied to form a diverse range of Si/metal oxide thermites for tailored applications.

METHODS

Synthesis of Si/Fe_2O_3 CS NPs. First, 100 mg of Si NPs was dispersed into 100 mL of isopropyl alcohol and sonicated for 15 min to break up the Si particle clusters. (3-Aminopropyl)-triethoxysilane (APTES, 1 mL, 99%, Sigma-Aldrich) and 0.5 mL of Milli-Q water were sequentially added to the Si NP solution and stirred at 70 °C for 1 h to functionalize the surface of Si with APTES. Second, the functionalized Si NPs were washed with deionized (DI) water and collected by centrifugation, and then, they were immersed in 40 mL of palladium chloride aqueous solution (20 mg of $PdCl_2$, Sigma-Aldrich, and 0.1 mL of reagent grade 37% HCl, Fisher Scientific) and stirred for 20 min. This electrostatic plating step coats the Si NPs with a thin layer of Pd film. Again, the Pd-coated Si NPs were washed with DI water and collected by centrifugation. The third step is to replace Pd with Fe by

DOI: 10.1021/acsomega.7b00652
ACS Omega 2017, 2, 3596–3600

Table 2. Comparison of Onset Temperatures of Different Thermites

sample	size of Si or Al (nm)	DSC heating rate (°C/min)	onset temperature (°C)	references
Si/Fe_2O_3 CS NPs	100	5	555	present work
Si/Fe_2O_3 CS NPs	100	10	551	present work
Si/Fe_2O_3 CS NPs	100	20	545	present work
Al/Fe_2O_3 xerogel nanocomposites	100	10	550	28
Al/Fe_2O_3 MM NPs	50	10	579	29
Al/Co_3O_4 nanocomposites	50	20	560	30
CuO/Al CS nanowires	100	5	549	9
Al/CuO MM NPs	80−150	10	460	31[a]
Al/Bi_2O_3 MM NPs	80−150	10	460	31[a]
Al/MoO_3 MM NPs	80−150	10	460	31[a]

[a]Might have used different definitions of onset temperature.

electroless plating. Specifically, the Pd-coated Si NPs were stirred for 5 min in 100 mL of DI water solution that contained 11.8 g of sodium citrate, 3.1 g of ammonium iron sulfate, 0.37 g of boric acid, 0.4 g of saccharin, and 0.1 g of lysine (all from Sigma-Aldrich). Then, 0.3 g of sodium borohydride (98%, Sigma-Aldrich) was added to the solution to initiate the electroless plating reaction. The resulted Si/Fe NPs were magnetic, so they were collected with a magnet. After rinsing with isopropyl alcohol and fully drying in vacuum, the Si/Fe NPs were annealed in a furnace in air at 450 °C for 5 h at a ramping time of 3 h. After annealing, the color of the NPs changed from black to red, indicating that the Fe shell was oxidized to Fe_2O_3.

DSC Measurement of Si/Fe_2O_3 CS and MM NPs. For a typical DSC measurement, a Si/Fe_2O_3 sample of about 5 mg (either CS or MM NPs) was placed in a 100 μL alumina crucible. The sample was heated in an inert argon environment (40 sccm) from room temperature to 900 °C at a heating rate of 5 °C/min. After the samples were cooled down to room temperature, they were heated with the same process again. The second-round heat flow traces were used to correct the baseline of the first-round heat flow traces following the method described previously.[25]

AUTHOR INFORMATION

Corresponding Author

*E-mail: xlzheng@stanford.edu. Phone: +1(650) 736-8953. Fax: +1(650) 723-1748 (X.Z.).

ORCID

Sidi Huang: 0000-0001-5703-0807
Sili Deng: 0000-0002-3421-7414
Jiheng Zhao: 0000-0001-8341-9031
Xiaolin Zheng: 0000-0002-8889-7873

Author Contributions

§S.H. and S.D. contributed equally to this work.

Notes

The authors declare no competing financial interest.

ACKNOWLEDGMENTS

This work was supported by Army Research Office under the agreement number W911NF-14-1-0271 and the Office of Naval Research under the agreement number N00014-15-1-2028. We would like to acknowledge Dr. Lei Liao for the helpful discussion on the electroless deposition method of Si/Fe_2O_3 CS NPs.

REFERENCES

(1) Wang, L. L.; Munir, Z. A.; Maximov, Y. M. Thermite Reactions: Their Utilization in the Synthesis and Processing of Materials. *J. Mater. Sci.* **1993**, *28*, 3693−3708.

(2) Orrù, R.; Sannia, M.; Cincotti, A.; Cao, G. Treatment and Recycling of Zinc Hydrometallurgical Wastes by Self-Propagating Reactions. *Chem. Eng. Sci.* **1999**, *54*, 3053−3061.

(3) Dreizin, E. L. Metal-Based Reactive Nanomaterials. *Prog. Energy Combust. Sci.* **2009**, *35*, 141−167.

(4) Gan, Y.; Qiao, L. Combustion Characteristics of Fuel Droplets with Addition of Nano and Micron-Sized Aluminum Particles. *Combust. Flame* **2011**, *158*, 354−368.

(5) Wang, J.; Qiao, Z.; Yang, Y.; Shen, J.; Long, Z.; Li, Z.; Cui, X.; Yang, G. Core−Shell Al-Polytetrafluoroethylene (PTFE) Configurations to Enhance Reaction Kinetics and Energy Performance for Nanoenergetic Materials. *Chem.—Eur. J.* **2016**, *22*, 279−284.

(6) Zhou, X.; Xu, D.; Yang, G.; Zhang, Q.; Shen, J.; Lu, J.; Zhang, K. Highly Exothermic and Superhydrophobic Mg/Fluorocarbon Core/Shell Nanoenergetic Arrays. *ACS Appl. Mater. Interfaces* **2014**, *6*, 10497−10505.

(7) Zhang, T.; Ma, Z.; Li, G.; Wang, Z.; Zhao, B.; Luo, Y. Electrostatic Interactions for Directed Assembly of High Performance Nanostructured Energetic Materials of Al/Fe_2O_3/Multi-Walled Carbon Nanotube (MWCNT). *J. Solid State Chem.* **2016**, *237*, 394−403.

(8) Séverac, F.; Alphonse, P.; Estève, A.; Bancaud, A.; Rossi, C. High-Energy Al/CuO Nanocomposites Obtained by DNA-Directed Assembly. *Adv. Funct. Mater.* **2012**, *22*, 323−329.

(9) Ohkura, Y.; Liu, S.-Y.; Rao, P. M.; Zheng, X. Synthesis and Ignition of Energetic CuO/Al Core/Shell Nanowires. *Proc. Combust. Inst.* **2011**, *33*, 1909−1915.

(10) Fischer, S.; Grubelich, M. *A Survey of Combustible Metals, Thermites, and Intermetallics for Pyrotechnic Applications*, 1996.

(11) Lafontaine, E.; Comet, M. *Nanothermites*; John Wiley & Sons, Inc.: Hoboken, NJ, USA, 2016.

(12) Thiruvengadathan, R.; Belarde, G. M.; Bezmelnitsyn, A.; Shub, M.; Balas-Hummers, W.; Gangopadhyay, K.; Gangopadhyay, S. Combustion Characteristics of Silicon-Based Nanoenergetic Formulations with Reduced Electrostatic Discharge Sensitivity. *Propellants, Explos., Pyrotech.* **2012**, *37*, 359−372.

(13) Yetter, R. A.; Risha, G. A.; Son, S. F. Metal Particle Combustion and Nanotechnology. *Proc. Combust. Inst.* **2009**, *32*, 1819−1838.

(14) Comet, M.; Siegert, B.; Schnell, F.; Pichot, V.; Ciszek, F.; Spitzer, D. Phosphorus-Based Nanothermites: A New Generation of Pyrotechnics Illustrated by the Example of n-CuO/Red P Mixtures. *Propellants, Explos., Pyrotech.* **2010**, *35*, 220−225.

(15) Comet, M.; Schnell, F.; Pichot, V.; Mory, J.; Risse, B.; Spitzer, D. Boron as Fuel for Ceramic Thermites. *Energy Fuels* **2014**, *28*, 4139−4148.

(16) Sullivan, K.; Young, G.; Zachariah, M. R. Enhanced Reactivity of Nano-B/Al/CuO MIC's. *Combust. Flame* **2009**, *156*, 302−309.

DOI: 10.1021/acsomega.7b00652
ACS Omega 2017, 2, 3596−3600

(17) Morita, M.; Ohmi, T.; Hasegawa, E.; Kawakami, M.; Ohwada, M. Growth of Native Oxide on a Silicon Surface. *J. Appl. Phys.* **1990**, *68*, 1272−1281.
(18) Terry, B. C.; Lin, Y.-C.; Manukyan, K. V.; Mukasyan, A. S.; Son, S. F.; Groven, L. J. The Effect of Silicon Powder Characteristics on the Combustion of Silicon/Teflon/Viton Nanoenergetics. *Propellants, Explos., Pyrotech.* **2014**, *39*, 337−347.
(19) Ledesma, H. A.; Tian, B. Nanoscale Silicon for Subcellular Biointerfaces. *J. Mater. Chem. B* **2017**, *5*, 4276−4289.
(20) Mason, B. A.; Groven, L. J.; Son, S. F.; Yetter, R. A. Combustion Performance of Several Nanosilicon-Based Nanoenergetics. *J. Propul. Power* **2013**, *29*, 1435−1444.
(21) Zhou, X.; Torabi, M.; Lu, J.; Shen, R.; Zhang, K. Nanostructured Energetic Composites: Synthesis, Ignition/Combustion Modeling, and Applications. *ACS Appl. Mater. Interfaces* **2014**, *6*, 3058−3074.
(22) Rossi, C.; Zhang, K.; Esteve, D.; Alphonse, P.; Tailhades, P.; Vahlas, C. Nanoenergetic Materials for MEMS: A Review. *J. Microelectromech. Syst.* **2007**, *16*, 919−931.
(23) Shimojo, F.; Nakano, A.; Kalia, R. K.; Vashishta, P. Electronic Processes in Fast Thermite Chemical Reactions: A First-Principles Molecular Dynamics Study. *Phys. Rev. E: Stat., Nonlinear, Soft Matter Phys.* **2008**, *77*, 066103.
(24) Mallory, G. O.; Hajdu, J. B. *Electroless Plating: Fundamentals and Applications*; William Andrew, 1990.
(25) Parimi, V. S.; Huang, S.; Zheng, X. Enhancing Ignition and Combustion of Micron-Sized Aluminum by Adding Porous Silicon. *Proc. Combust. Inst.* **2017**, *36*, 2317−2324.
(26) Silicon (Si) Nanopowder/Nanoparticles (Si, 98+%, 20−30 nm, Laser Synthesized, Polycrystalline Structure). http://www.us-nano.com/inc/sdetail/374 (accessed Jun 28, 2017).
(27) Nanomaterials, S. Nano Powder, Copper Nanoparticles, Lanthanum Oxide, Nano Powders, Titanium Nanoparticles. http://ssnano.com/inc/sdetail/silicon-nanoparticles-99--100-nm/147/291 (accessed Jun 28, 2017).
(28) Shin, M.-S.; Kim, J.-K.; Kim, J.-W.; Moraes, C. A. M.; Kim, H.-S.; Koo, K.-K. Reaction Characteristics of Al/Fe_2O_3 Nanocomposites. *J. Ind. Eng. Chem.* **2012**, *18*, 1768−1773.
(29) Zhao, N.; He, C.; Liu, J.; Gong, H.; An, T.; Xu, H.; Zhao, F.; Hu, R.; Ma, H.; Zhang, J. Dependence of Catalytic Properties of Al/Fe_2O_3 Thermites on Morphology of Fe_2O_3 Particles in Combustion Reactions. *J. Solid State Chem.* **2014**, *219*, 67−73.
(30) Zhang, D.; Xiang, Q. Electrophoretic Fabrication of an Al−Co_3O_4 Reactive Nanocomposite Coating and Its Application in a Microignitor. *Ind. Eng. Chem. Res.* **2016**, *55*, 8243−8247.
(31) Glavier, L.; Taton, G.; Ducéré, J.-M.; Baijot, V.; Pinon, S.; Calais, T.; Estève, A.; Rouhani, M. D.; Rossi, C. Nanoenergetics as Pressure Generator for Nontoxic Impact Primers: Comparison of Al/Bi2O3, Al/CuO, Al/MoO3 Nanothermites and Al/PTFE. *Combust. Flame* **2015**, *162*, 1813−1820.

DOI: 10.1021/acsomega.7b00652
ACS Omega 2017, 2, 3596−3600